

Charge doping effects on magnetic properties of single-crystal $\text{La}_{1-x}\text{Sr}_x(\text{Cr}_{0.2}\text{Mn}_{0.2}\text{Fe}_{0.2}\text{Co}_{0.2}\text{Ni}_{0.2})\text{O}_3$ ($0 \leq x \leq 0.5$) high-entropy perovskite oxides

Alessandro R. Mazza,¹ Elizabeth Skoropata¹, Jason Lapano¹, Jie Zhang,¹ Yogesh Sharma,^{1,2} Brianna L. Musico,³ Veerle Keppens³, Zheng Gai⁴, Matthew J. Brahlek,¹ Adriana Moreo,^{1,5} Dustin A. Gilbert,³ Elbio Dagotto,^{1,5} and Thomas Z. Ward^{1,*}

¹Materials Science and Technology Division, Oak Ridge National Laboratory, Oak Ridge, Tennessee 37831, USA

²Center for Integrated Nanotechnologies, Los Alamos National Laboratory, Los Alamos, New Mexico 87545, USA

³Department of Materials Science and Engineering, University of Tennessee, Knoxville, Tennessee 37996-4545, USA

⁴Center for Nanophase Materials Sciences, Oak Ridge National Laboratory, Oak Ridge, Tennessee 37831, USA

⁵Department of Physics and Astronomy, University of Tennessee, Knoxville, Tennessee 37996, USA



(Received 30 April 2021; revised 2 July 2021; accepted 1 September 2021; published 15 September 2021)

The influence of hole doping on magnetic properties is mapped for the compositionally complex high-entropy oxide ABO_3 perovskite $\text{La}_{1-x}\text{Sr}_x(\text{Cr}_{0.2}\text{Mn}_{0.2}\text{Fe}_{0.2}\text{Co}_{0.2}\text{Ni}_{0.2})\text{O}_3$ ($0 \leq x \leq 0.5$). It is found that aliovalent A -site substitution is a viable means to manipulate the magnetically active B -site sublattice. A series of single-crystal films are synthesized and show a general trend toward stronger ferromagnetic response and a shift in magnetic anisotropy as the Sr concentration increases. Magnetometry demonstrates complex and nonuniform responses similar to rigid and uncoupled composites at intermediate dopings. This behavior points to the presence of locally inhomogeneous magnetic phase competition, where ferromagnetic and antiferromagnetic magnetic contributions create a frustrated matrix containing uncompensated spins at the boundaries between these regions. The observations are discussed in the context of known responses to hole doping in the less complex ternary LaT_MO_3 ($T_M = \text{Cr, Mn, Fe, Co, Ni}$) oxides, and they are found to be different from a simple sum of the doped parents. The results are summarized in a preliminary magnetic phase diagram.

DOI: [10.1103/PhysRevB.104.094204](https://doi.org/10.1103/PhysRevB.104.094204)

I. INTRODUCTION

Local elemental diversity and the accompanying combination of site-to-site interactions dictate the global phase and functionality of materials. However, the role of these microstates is often beholden to very small amounts of doping so as to avoid disrupting crystallinity. Recent developments in entropy-assisted synthesis are allowing an extraordinary increase in the number of microstates present on uniform crystal lattices [1–3], where five or more elements can be hosted and well-mixed on a single sublattice despite the massive amount of site-to-site disorder. This method of creating high entropy oxides (HEOs) is still in its infancy, but it appears to be a generally viable approach that can be applied to many different crystal structures, including spinel [4,5], perovskite [6,7], Ruddlesden-Popper [8], and rocksalt [9–11]. Mechanistically, the complex set of local microstates present in these systems is suggested as the driving influence that leads to unexpected and often exceptional properties related to magnetism [4,5,7,11–13], ion conductivity [14–16], catalytic tunability [17], thermal transport [6,18], and electronic character [19]. These observations promise the ability to access never before possible combinations of diverse local interactions on uniform crystal lattices that are likely to lead to new physical behaviors. However, due to the innate complexity

present, gaining a general fundamental understanding of these chaotically populated systems is challenging. For this reason, it is important to work toward identifying how slight and iterative manipulation of the local interaction landscape works to drive the emergence of macroscopic functional responses.

The ABO_3 perovskites host two cation sublattices, and they are well-studied in ternary compounds. In strongly correlated transition-metal oxide (TMO) perovskites, such as LaT_MO_3 ($T_M = \text{Cr, Mn, Fe, Co, Ni}$), the B -site sublattice generally acts as the magnetically and electronically dominant sublattice, where slight changes to the B -site charge state, coordination, or bond symmetry can dictate the functional properties. A conventional approach to interrogate and control these phases is to use the A -site sublattice to impart changes on the functionally active B -sites. As an example, substitutional doping on the A -site can be used to shift the local charge, spin, and exchange interactions of the neighboring B -sites. In the case of the TMOs, iterative doping studies are often conducted to gain general insights into how changes to the microstate might drive macroscopic responses. This often results in the revelation of rich phase diagrams such as that seen in $\text{La}_{1-x}\text{Sr}_x\text{MnO}_3$ (LSMO), where various types of magnetic, orbital, electronic, and structural order can be observed [20]. Here, iteratively replacing the La^{3+} with Sr^{2+} drives charge compensation on the B -site Mn, which can lead to the opening of $\text{Mn}^{3+}\text{-O}^{2-}\text{-Mn}^{4+}$ double exchange pathways and ferromagnetism from the parent antiferromagnetic (AFM) state [21]. Similarly, in $\text{La}_{1-x}\text{Sr}_x\text{CoO}_3$ (LSCO), Co^{3+}

*wardtz@ornl.gov

is pushed from the low-spin state to the high-spin Co^{4+} state, which initiates a ferromagnetic (FM) phase transition [22]. Conversely, $\text{La}_{1-x}\text{Sr}_x\text{CrO}_3$ and $\text{La}_{1-x}\text{Sr}_x\text{FeO}_3$ remain AFM with hole doping and only show a drop in ordering temperature with increasing Sr concentration [23–25]. In these previous works, hole doping experiments helped to clarify the fundamental mechanisms driving functionality and led to the discovery of unexpected and novel behaviors. Extending this systematic process to configurationally complex materials may then provide important insights that can help guide our understanding of the mechanisms driving this unexplored class of materials.

$\text{La}(\text{Cr}_{0.2}\text{Mn}_{0.2}\text{Fe}_{0.2}\text{Co}_{0.2}\text{Ni}_{0.2})\text{O}_3$ (LS5BO) is a compositionally complex perovskite oxide that demonstrates interesting magnetic and structural responses in which large amounts of spin and magnetic exchange disorder lead to extraordinary diversity of microstates [12,26,27]. In this work, modification of these local states through hole doping is found to provide a means of controlling magnetic phase and anisotropy. The doping experiments rely on substitutional doping on the A-site sublattice and are found to have no adverse effect on crystal quality. X-ray diffraction and reflectivity measurements show that all films are single-phase, coherently strained, epitaxial to the substrate, and possess low surface roughness. Crystalline quality is vital to investigations into fundamental magnetic processes, as this reduces possible extrinsic effects such as grain boundaries and structural inhomogeneities that are present in ceramic and powder samples. Through magnetometry measurements, hole doping is found to provide a means of controlling the FM bonds in $\text{La}_{1-x}\text{Sr}_x(\text{Cr}_{0.2}\text{Mn}_{0.2}\text{Fe}_{0.2}\text{Co}_{0.2}\text{Ni}_{0.2})\text{O}_3$ ($0 \leq x \leq 0.5$) (LS5BO) films. The increasing phase fraction of ferromagnetism is found to coincide with a change in its blocking temperature, which indicates smaller average domain sizes with increasing Sr. At low doping, there is a locally inhomogeneous magnetic phase competition, where uncoupled soft (uncompensated moments) and hard magnetic contributions preclude direct coupling of AFM and FM magnetic regions. The coupling of these phases is found to be tunable with Sr doping.

II. METHODS

Stoichiometric ceramic targets for each of the LS5BO compositions are prepared via conventional solid-state reaction at 1000 °C. Films are grown via pulsed laser deposition on SrTiO_3 (0,0,1) substrates using a KrF excimer laser at a fluence of 0.85 J/cm^2 and a repetition rate of 5 Hz with oxygen partial pressure held at 90 mTorr for all samples. Substrate temperature during growth is composition-dependent and held at 625, 635, 635, and 700 °C for Sr 0%, 10%, 30%, and 50%, respectively. All films are cooled from growth conditions under 200 Torr oxygen pressure.

XRD and XRR measurements are performed using a four-circle high-resolution x-ray diffractometer utilizing $\text{Cu } K\alpha_1$ radiation (Panalytical X'Pert Pro). Magnetization measurements conducted on a Quantum Design MPMS3 magnetometer are corrected for substrate background by subtracting the diamagnetic background signal from collected data.

III. RESULTS AND DISCUSSION

A series of single-crystal LS5BO films are grown with $x = 0, 0.1, 0.3,$ and 0.5 with a typical thickness of $\sim 50 \text{ nm}$. These samples are designated by their Sr concentration on the A-site sublattice as Sr 0%, 10%, 30%, and 50% for x values 0, 0.1, 0.3, and 0.5, respectively. Figure 1(a) shows the (0 0 2) diffraction scans revealing single crystals with no secondary phases and high crystalline uniformity inferred from well-defined Laue fringes. The film thickness determined from the Laue fringes (crystalline thickness) in each case matches the thickness determined from XRR (total thickness), giving strong evidence that phase segregation does not occur in the films. Each film's roughness is $< 3 \text{ nm}$ over the $5 \text{ mm} \times 5 \text{ mm}$ area, which is comparable to the expected roughness from the miscut angle of the substrate [Fig. 1(b)]. The in-plane lattice parameter of the films relative to the STO substrate is revealed from reciprocal space maps about the (1 1 3) peaks. From Fig. 1(c), it is evident that in each case the films are coherently strained. As a function of Sr doping, the lattice size contracts as expected from the smaller atomic size of Sr relative to La. Given the results of this characterization, the evolution of the c -axis size is shown in Fig. 1(d), where the gradual contraction of the c -axis with increasing Sr is quantified. It should be noted that the strain of each film was slightly different due to the contraction in the unit-cell size; this strain (c/a ratio) is also given in Fig. 1(d).

The temperature-dependent magnetization for all films is presented in Fig. 2. Here, the zero-field-cooled (ZFC) and field-cooled (FC) responses are shown with the magnetic field applied in both the in-plane (IP) and out-of-plane (OOP) directions. In all cases, the magnetic transitions appear uniform with clear onset temperatures. This single transition response signals a global phase change. Had chemical segregation or structural clustering been present, these magnetization curves would present multiple transitions as a sum of local regions similarly to that observed in HEO powders and ceramics [27]. This is an important advantage of conducting these studies on the single-crystal form; it is possible to investigate the inherent magnetic responses without the complications of extrinsic contributions present in materials with grain boundaries, large relative surface contributions, and size effects seen in polycrystalline and powder samples.

A general trend toward increasing FM character with increasing Sr is evident when looking at the uniformity of moment onsets as a function of temperature. Sr 0% and Sr 10% crystals both have a similar ferromagnetic blocking temperature (T_B), which is signaled by the opening of a gap between the FC and ZFC curves, at $\sim 175 \text{ K}$. The FM T_B coincides with the thermal energy barrier blocking the alignment of moments at low temperature. It can be affected by several features, including the magnitude of the applied field, anisotropy (K_u), and domain size. Considering that the applied field is constant for each sample, the size of the FM domains should correlate with T_B , which allows for qualitative comparison of the expected FM cluster sizes as a function of doping level. However, it is worth noting that the K_u increases with substitutional doping due to lattice strain, which can increase the effective T_B . In the Sr 30%, a similar transition to that seen in the Sr 0% and 10% appears, but a kink at $\sim 50 \text{ K}$ arises in

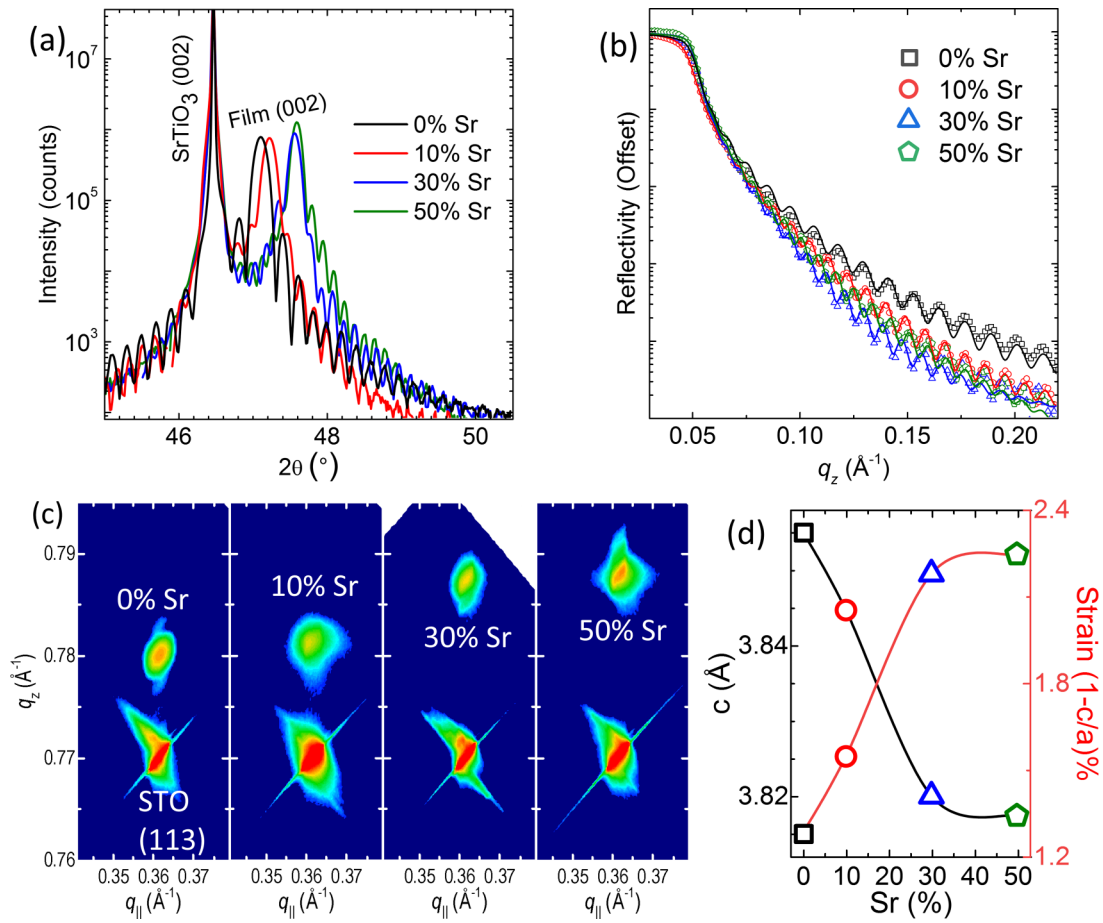


FIG. 1. X-ray diffraction and reflectivity studies for all films. (a) XRD showing the (0 0 2) peak demonstrating high crystalline quality of films. (b) XRR data for each of the films demonstrating low surface roughness. (c) RSM data showing films are fully strained to the substrate. (d) Evolution of the c -axis lattice parameter and corresponding lattice strain.

the IP configuration. This feature persists in the Sr 50% where only this sharp transition is observed. This is consistent with a transition from a soft ferromagnet (or paramagnet) to a hard FM phase. The lowering of T_B , despite the increased K_u due to increasing crystalline strain, which is expected to increase T_B , with increasing Sr suggests that the size of the FM clusters is decreasing. This is different from doping trends observed in ternary parents to the L5BO, such as $\text{La}_{1-x}\text{Sr}_x\text{MnO}_3$, which show an increase in cluster size across this doping range.

The FM nature of the films is further investigated by measuring magnetization as a function of applied magnetic field at various temperatures for each Sr concentration. Figure 3 presents representative field loops taken at 10, 25, 100, and 250 K for each doping. By comparison of the IP loops [Figs. 3(a)–3(d)], the saturation magnetization (M_s) increases with Sr concentration at low temperature. This is especially evident as Sr concentration moves from 0% toward 30%, where both Sr 30% and Sr 50% saturate around $0.2\mu_B/\text{unit cell}$ (u.c.). In addition, increasing hole doping toward the highest levels induces a much larger coercivity, though the loops at 10 K do not fully saturate. Turning to the OOP direction [Figs. 3(e)–3(h)], each of the concentrations exhibits a higher coercivity and M_s (approaching $0.3\mu_B/\text{u.c.}$ for Sr 30% and Sr 50%) than their IP loops. This points to the FM component having an easy axis in the OOP direction

for each of the films. The magnetic hysteresis loops and the temperature dependence led to the conclusion that increasing Sr concentration results in increasing M_s and K_u , while simultaneously decreasing T_B . These results taken together again indicate that, as Sr concentration increases, the size of the FM clusters is decreasing while simultaneously increasing in number or absolute moment. The presence of FM clusters existing in a background AFM matrix should produce uncompensated or frustrated spins along the cluster walls. If present, changes to domain boundary compositions would leave signatures in the macroscopic temperature-dependent coercivities and hysteretic responses [28–30].

The temperature dependence of the IP coercivity is shown in Fig. 4 for each Sr concentration. Coercivity increases as temperature is reduced for the Sr 30% and Sr 50% films. This behavior, when taken with the other observations, points to the coexistence of FM and AFM regions in these films. Here, percolated FM regions can be coupled to the AFM phase domains through magnetic exchange, where uncompensated spins at boundaries appear to decrease with increasing Sr [31,32]. Coercivity also increases for the Sr 0% and Sr 10% films as temperature drops below the blocking temperature; however, the coercivity falls at low temperatures. This reduction of coercivity can be the result of an increase in FM cluster size. This is enabled by domain propagation between

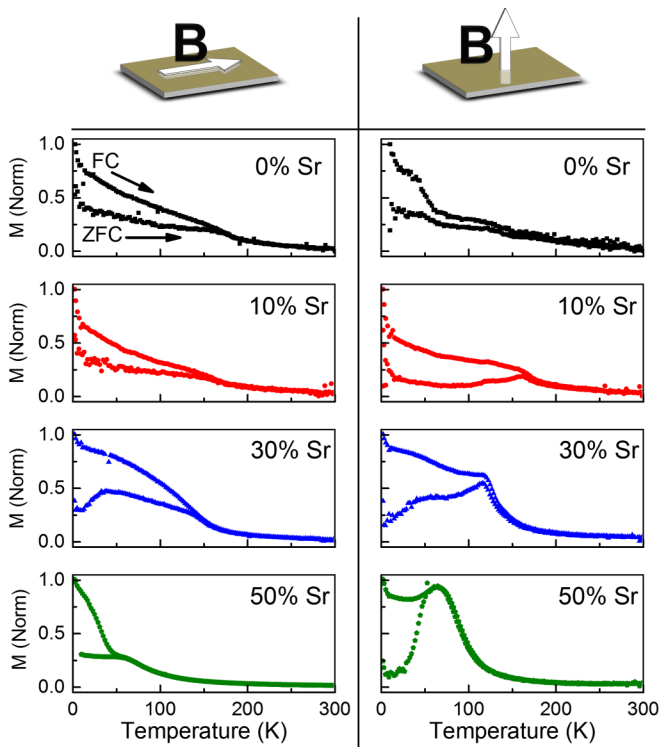


FIG. 2. Field-cooled and zero-field-cooled magnetization as a function of temperature on warming under 1000 Oe field for all compositions. In all cases, magnetic transitions are consistent with a macroscopically coherent ordering and not the result of small pockets that correlate to parent phase transitions.

clusters, which will produce a lower coercivity in comparison to isolated FM clusters. Conversely, this may be due to local pinning of uncompensated moments at the frustrated magnetic boundary between AFM and FM regions. This leaves the question of how the phase coexistence and interdomain couplings evolve to influence the complex loop shapes and decreased coercivity observed in the lower dosed Sr 0% and Sr 10% crystals.

Figure 5 provides a more in-depth look at how magnetic responses change as low concentrations of Sr are introduced by comparing undoped (Sr 0%) and low doped (Sr 10%) materials. At temperatures above 15 K, we observe the emergence of complicated magnetic responses that are consistent with coexisting but uncoupled magnetic phases. In the 0% sample, a soft magnetic component is superimposed on a linear field-dependent moment suggesting a soft FM phase coexisting with a paramagnetic or weak and unsaturated AFM phase. Magnetic phases appear to harden below 15 K and become dominated by a more conventional FM response. In the Sr 10% case, the soft component saturates as one might expect from a soft ferromagnet or superparamagnet, but again this soft component does not appear to couple to the hard component. This is particularly clear at 50 K, where the soft loop switches near the zero-field crossing without impacting the hard component. Previous work on $\text{La}(\text{Cr}_{0.2}\text{Mn}_{0.2}\text{Fe}_{0.2}\text{Co}_{0.2}\text{Ni}_{0.2})\text{O}_3$ has shown the coexistence of AFM and FM orders that can lead to unusual exchange biasing responses manifesting as a vertical shift in magneti-

zation loop under field cooling, which also coincides with a decrease in coercivity [33]. The evolution of the hysteresis loops observed in this work suggests that there exists a soft magnetic component at the boundary region between FM and AFM phases at higher temperatures that transitions a sharper coupled boundary as energy is reduced at low temperatures. The soft component becomes rigid, likely influenced by coupling to the hard component, which gives rise to a uniform coercivity. This understanding provides an explanation for the drop in coercivity coinciding with the change in loop shape—an effect that would be expected with a growth in the size of the FM region through coupling to the soft magnetic component at the interface between AFM and FM portions of the film.

The mixed-magnetic phase response observed in the 0% and 10% samples can occur when soft (low coercivity) and hard (high coercivity) magnetic regions coexist in a material. A simplified example is illustrated in Fig. 6. Here, the soft portion of the film rotates with field while the hard component, subject to its coercivity, lags. This is represented in the illustration where the local moments in each of the components are shown for various portions of the uncoupled magnetic components contributing to the loop. The wasp-waisted hysteresis loops, observed in the OOP direction for Sr 0% and 10% cases, are the first indication of noteworthy interplay between the different magnetic phases in the films. Prior to this work, FM and AFM phases were known to exist in L5BO. However, the emerging multicomponent loops confirm the presence of a third contribution to the magnetic phase. The third contribution is attributed to the boundary between FM and AFM phases in the film where uncompensated spins can emerge. This creates a frustrated magnetization having an apparent PM-like or soft FM-like loop response to field that can be entirely decoupled from the FM clusters in the film.

Unlike the Sr 0% and Sr 10% crystals, the magnetization loops for the Sr 30% and 50% crystals are dominated by a FM component that gives no sign of the soft/hard mixed magnetic phases. The magnetic anisotropy for these higher Sr concentrations dictates the easy axis of magnetization and increased coercivity in the out-of-plane direction. When the magnetic field is applied in-plane, the FM component is extremely soft at intermediate temperatures until being purely PM above the FM blocking temperature. While the FM component increases for these higher concentrations, the relatively low M_s ($\sim 10\%$ of the total possible moment) and the expected presence of local AFM exchange couplings between some of the transition elements suggest that AFM order is still a dominant feature in these films.

From the observations above, a phenomenological phase diagram is constructed for $\text{La}_{1-x}\text{Sr}_x(\text{Cr}_{0.2}\text{Mn}_{0.2}\text{Fe}_{0.2}\text{Co}_{0.2}\text{Ni}_{0.2})\text{O}_3$ ($0 \leq x \leq 0.5$) in Fig. 7. The magnetic frustration is most prevalent at 10% Sr where the presence of uncompensated moments—behaving as a soft FM—in addition to an emerging hard FM portion of the film both contribute on a similar scale to the magnetization. This generates a loop shape exhibiting two uncoupled phases which become rigidly coupled at low temperature. A shift towards a dominant FM order with increasing Sr concentration likely couples to an increase in the average

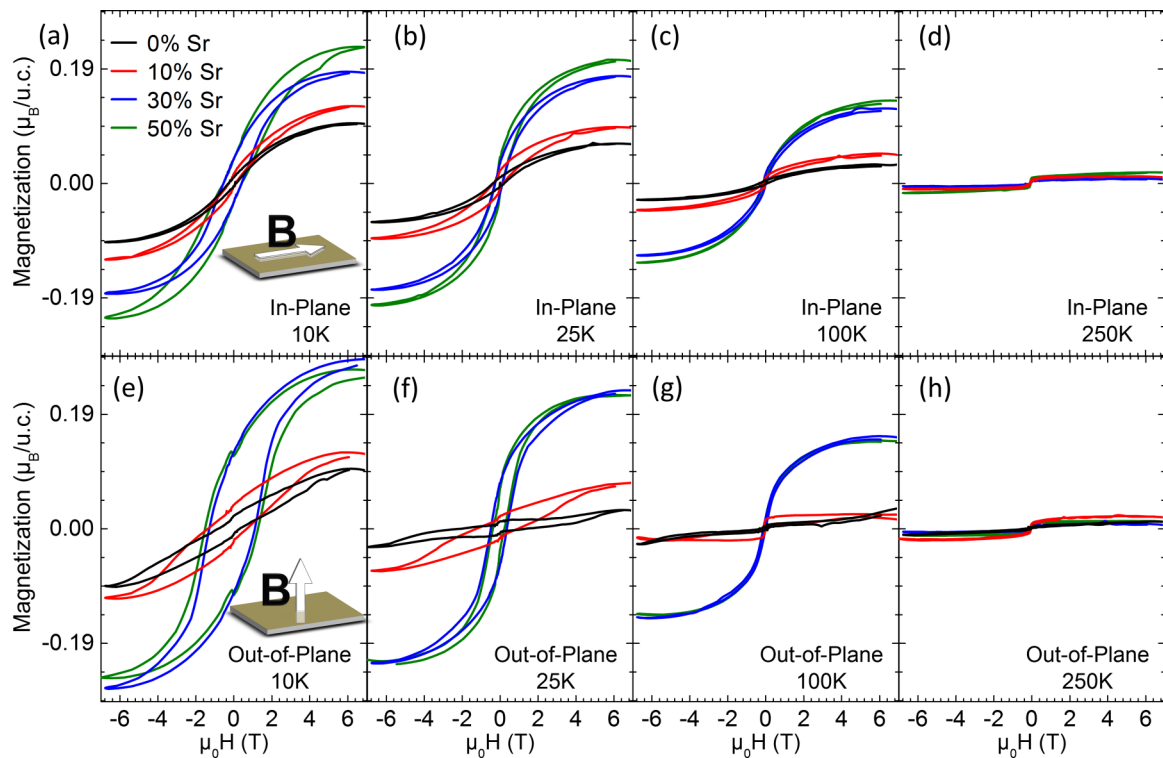


FIG. 3. Examples of field-dependent magnetic responses for different Sr compositions at 10, 25, 100, and 250 K for field applied in-plane (a)–(d) and out-of-plane (e)–(h).

valence of the transition metal on the *B*-site sublattice. This is suggested by a shift towards FM, which has been seen with the parent oxides $LaCoO_3$ and $LaMnO_3$ and through a gradual transition to lower Néel temperatures in $LaCrO_3$ and $LaFeO_3$ [22–25,34,35]. Ni^{4+} is considered an exotic charge state for Ni, so there are no examples of high-quality hole-doped $LaNiO_3$. This suggests that the entropy stabilization process may enable charge compensation in the easier to oxidize Mn, Cr, and Co. How charge compensation ties to crystal phase formation and stability in configurationally complex oxides

such as these is an open question at present. Given the clear transition towards ferromagnetism, it is likely that a shift towards Mn^{4+} and Co^{4+} enables double exchange pathways, which drives the observed increase in the FM volume fraction as Sr concentration increases. A crude approximation of this effect, which was used to model $(La, Sr)MnO_3$ [36], is the local enhancement of ferromagnetism at lattice sites near Sr. If we consider this model of double exchange in the LS5BO system, we have observed the emergence of robust but local FM clusters with increasing Sr, which mimics the

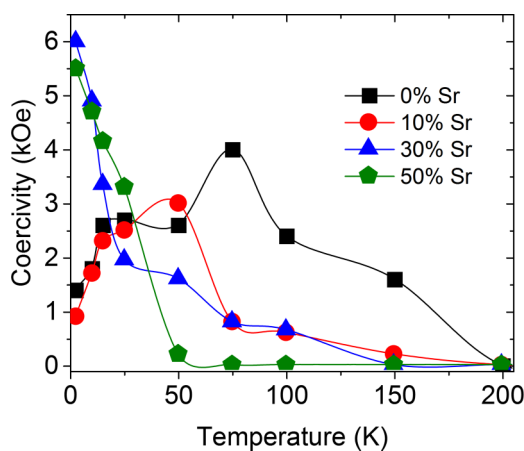


FIG. 4. A comparison of in-plane magnetic coercivity with temperature shows a drop in coercivity with temperature for low Sr concentrations and an increase in coercivity for higher Sr concentrations.

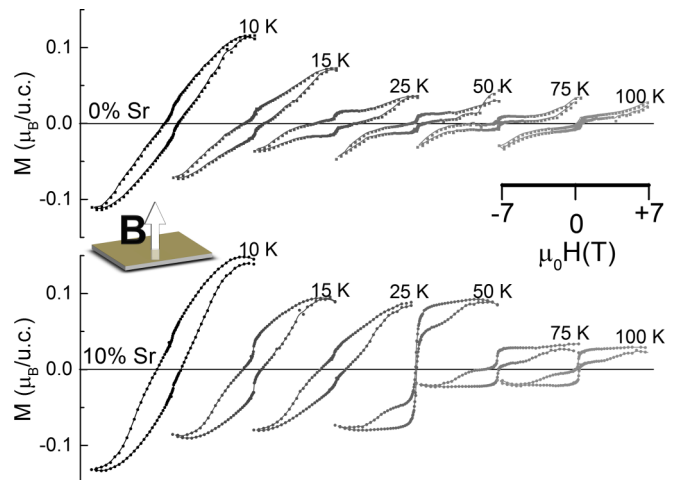


FIG. 5. Evolution of out-of-plane magnetization for Sr 0% (top) and Sr 10% (bottom) films shows that low concentrations of Sr can induce an uncoupled magnetic response.

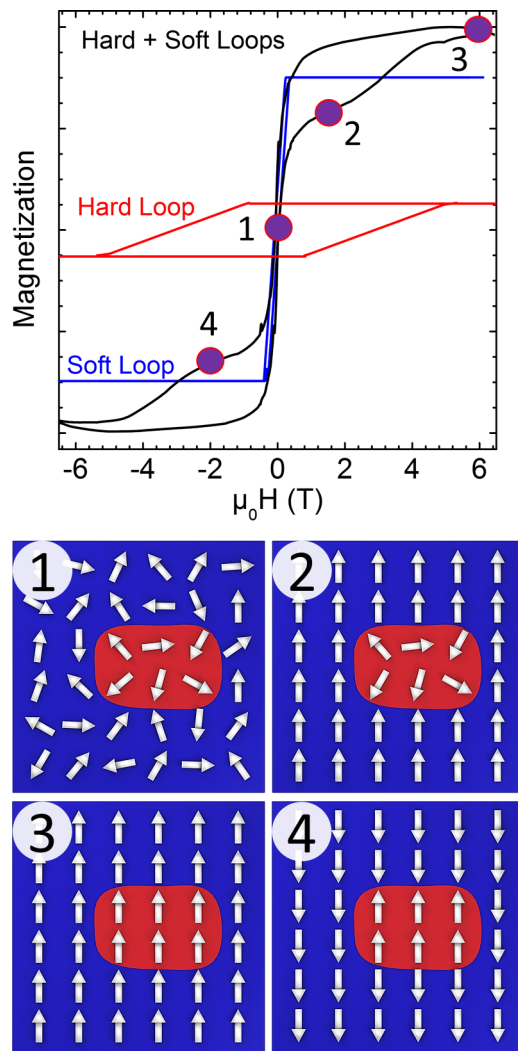


FIG. 6. The addition of hard and soft loops leading to exchange spring behavior (top) with a micromagnetic cartoon (bottom) representation of behavior of local competing magnetic responses along the experimental loop as field is swept from zero field (1) to high positive field (2–3) and then to intermediate negative field (4).

experimental result. This explanation is also consistent with the observation that the soft magnetic behavior critical to the two-phase loop shape in Sr 0% and Sr 10% samples begins to disappear as the FM phase becomes more dominating in the Sr 30% and Sr 50% compositions. However, the remaining difficulty is in understanding the observed decrease in T_B , which couples to a decrease in FM domain size. For this, we see two possible scenarios: (i) the loss of the glassy region of uncompensated moments decreases the effective FM size as these moments can couple to the ferromagnetism, or (ii) the change in charge state, while enabling double exchange in some cases, may diminish ferromagnetism in others. For example, while $\text{Fe}^{3+}\text{-O-Mn}^{3+}$ is known to give rise to ferromagnetism, $\text{Fe}^{3+}\text{-O-Mn}^{4+}$ may not. Future x-ray

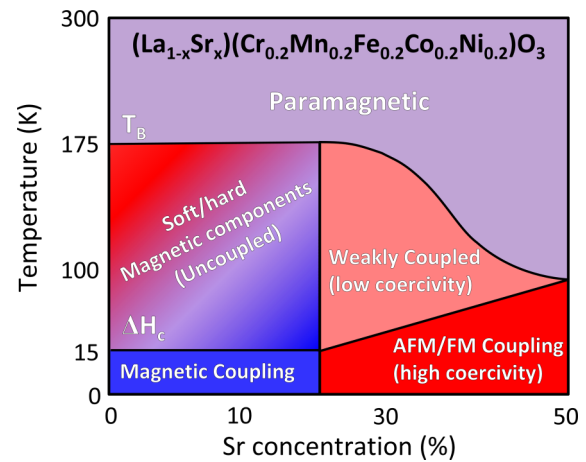


FIG. 7. Proposed magnetic phase diagram for the LS5BO system. The temperatures are chosen based on the blocking temperature (T_B) of the FM component and the change in coercivity (ΔH_c) at low temperature.

absorption spectroscopy and circular dichroism studies may shed light on which of these scenarios drives function.

Utilizing the traditional method of substitutional doping, the fundamental properties of configurationally complex materials are described. Hole doping does not have an adverse effect on the crystallinity of the high entropy oxide films. Through hole doping, it is found that the magnetic phase can be tuned—both increasing M_s and decreasing T_B . The magnetic responses are consistent with the presence of FM clusters, which grow in number (as evident from M_s) but decrease in size (as evident from T_B). From these results, a proposed phase diagram of an entropy-stabilized oxide is provided, paving the way for exploration of this rapidly expanding materials class.

ACKNOWLEDGMENTS

Experiment design, sample synthesis, structural characterization, and computational modeling were supported by the U.S. Department of Energy (DOE), Office of Basic Energy Sciences (BES), Materials Sciences and Engineering Division. B.L.M. thanks the Center for Materials Processing, a Center of Excellence at the University of Tennessee, Knoxville funded by the Tennessee Higher Education Commission (THEC), for financial support. This research used resources of the Advanced Photon Source, a U.S. Department of Energy (DOE) Office of Science User Facility operated for the DOE Office of Science by Argonne National Laboratory under Contract No. DE-AC02-06CH11357. Some SQUID magnetometry was performed as a user project at the Center for Nanophase Materials Sciences, which is sponsored at Oak Ridge National Laboratory (ORNL) by the Scientific User Facilities Division, BES, DOE. Some neutron diffraction experiments were conducted at the Spallation Neutron Source, a DOE Office of Science User Facility operated by the Oak Ridge National Laboratory.

- [1] N. Dragoë and D. Bérardan, Order emerging from disorder, *Science* **366**, 573 (2019).
- [2] A. Sarkar, B. Breitung, and H. Hahn, High entropy oxides: The role of entropy, enthalpy and synergy, *Scr. Mater.* **187**, 43 (2020).
- [3] C. M. Rost, E. Sachet, T. Borman, A. Moballeggh, E. C. Dickey, D. Hou, J. L. Jones, S. Curtarolo, and J.-P. Maria, Entropy-stabilized oxides, *Nat. Commun.* **6**, 8485 (2015).
- [4] A. Mao, H.-Z. Xiang, Z.-G. Zhang, K. Kuramoto, H. Zhang, and Y. Jia, A new class of spinel high-entropy oxides with controllable magnetic properties, *J. Magn. Magn. Mater.* **497**, 165884 (2020).
- [5] J. Dąbrowa, M. Stygar, A. Mięka, A. Knapik, K. Mroczka, W. Tejchman, M. Danielewski, and M. Martin, Synthesis and microstructure of the (Co, Cr, Fe, Mn, Ni)₃O₄ high entropy oxide characterized by spinel structure, *Mater. Lett.* **216**, 32 (2018).
- [6] Y. Sharma, B. L. Musico, X. Gao, C. Hua, A. F. May, A. Herklotz, A. Rastogi, D. Mandrus, J. Yan, H. N. Lee, M. F. Chisholm, V. Keppens, and T. Z. Ward, Single-crystal high entropy perovskite oxide epitaxial films, *Phys. Rev. Mater.* **2**, 060404(R) (2018).
- [7] A. Sarkar, R. Djenadic, D. Wang, C. Hein, R. Kautenburger, O. Clemens, and H. Hahn, Rare earth and transition metal based entropy stabilised perovskite type oxides, *J. Eur. Ceram. Soc.* **38**, 2318 (2018).
- [8] W. Zhang, A. R. Mazza, E. Skoropata, D. Mukherjee, B. Musico, J. Zhang, V. M. Keppens, L. Zhang, K. Kisslinger, E. Stavitski, M. Brahlek, J. W. Freeland, P. Lu, and T. Z. Ward, Applying configurational complexity to the 2D Ruddlesden-Popper crystal structure, *ACS Nano* **14**, 13030 (2020).
- [9] C. M. Rost, Z. Rak, D. W. Brenner, and J.-P. Maria, Local structure of the Mg_xNi_xCo_xCu_xZn_xO ($x = 0.2$) entropy-stabilized oxide: An exafs study, *J. Am. Ceram. Soc.* **100**, 2732 (2017).
- [10] B. L. Musico, D. Gilbert, T. Z. Ward, K. Page, E. George, J. Yan, D. Mandrus, and V. Keppens, The emergent field of high entropy oxides: Design, prospects, challenges, and opportunities for tailoring material properties, *APL Mater.* **8**, 040912 (2020).
- [11] J. Zhang, J. Yan, S. Calder, Q. Zheng, M. A. McGuire, D. L. Abernathy, Y. Ren, S. H. Lapidus, K. Page, H. Zheng, J. W. Freeland, J. D. Budai, and R. P. Hermann, Long-range antiferromagnetic order in a rocksalt high entropy oxide, *Chem. Mater.* **31**, 3705 (2019).
- [12] Y. Sharma, Q. Zheng, A. R. Mazza, E. Skoropata, T. Heitmann, Z. Gai, B. Musico, P. F. Miceli, B. C. Sales, V. Keppens, M. Brahlek, and T. Z. Ward, Magnetic anisotropy in single-crystal high-entropy perovskite oxide La(Cr_{0.2}Mn_{0.2}Fe_{0.2}Co_{0.2}Ni_{0.2})O₃ films, *Phys. Rev. Mater.* **4**, 014404 (2020).
- [13] P. B. Meisenheimer, T. J. Kratořil, and J. T. Heron, Giant enhancement of exchange coupling in entropy-stabilized oxide heterostructures, *Sci. Rep.* **7**, 13344 (2017).
- [14] D. Bérardan, S. Franger, A. K. Meena, and N. Dragoë, Room temperature lithium superionic conductivity in high entropy oxides, *J. Mater. Chem. A* **4**, 9536 (2016).
- [15] A. Sarkar, L. Velasco, D. Wang, Q. Wang, G. Talasila, L. de Biasi, C. Kübel, T. Brezesinski, S. S. Bhattacharya, H. Hahn, and B. Breitung, High entropy oxides for reversible energy storage, *Nat. Commun.* **9**, 3400 (2018).
- [16] A. Sarkar, Q. Wang, A. Schiele, M. R. Chellali, S. S. Bhattacharya, D. Wang, T. Brezesinski, H. Hahn, L. Velasco, and B. Breitung, High-entropy oxides: Fundamental aspects and electrochemical properties, *Adv. Mater.* **31**, 1806236 (2019).
- [17] H. Chen, J. Fu, P. Zhang, H. Peng, C. W. Abney, K. Jie, X. Liu, M. Chi, and S. Dai, Entropy-stabilized metal oxide solid solutions as CO oxidation catalysts with high-temperature stability, *J. Mater. Chem. A* **6**, 11129 (2018).
- [18] J. L. Braun, C. M. Rost, M. Lim, A. Giri, D. H. Olson, G. N. Kotsonis, G. Stan, D. W. Brenner, J.-P. Maria, and P. E. Hopkins, Charge-induced disorder controls the thermal conductivity of entropy-stabilized oxides, *Adv. Mater.* **30**, 1805004 (2018).
- [19] D. Bérardan, S. Franger, D. Dragoë, A. K. Meena, and N. Dragoë, Colossal dielectric constant in high entropy Oxides, *Phys. Status Solidi RRL–Rapid Res. Lett.* **10**, 328 (2016).
- [20] J. Hemberger, A. Krimmel, T. Kurz, H.-A. Krug von Nidda, V. Yu. Ivanov, A. A. Mukhin, A. M. Balbashov, and A. Loidl, Structural, magnetic, and electrical properties of single-crystalline La_{1-x}Sr_xMnO₃ ($0.4 < x < 0.85$), *Phys. Rev. B* **66**, 094410 (2002).
- [21] M. B. Salamon and M. Jaime, The physics of manganites: structure and transport, *Rev. Mod. Phys.* **73**, 583 (2001).
- [22] V. V. Sikolenko, A. P. Sazonov, I. O. Troyanchuk, D. Többsen, U. Zimmermann, E. V. Pomjakushina, and H. Szymczak, Magnetic properties of La_{1-x}Sr_xCoO₃ ($x = 0.15$ and 0.3), *J. Phys. Condens. Matter* **16**, 7313 (2004).
- [23] K. Tezuka, Y. Hinatsu, A. Nakamura, T. Inami, Y. Shimojo, and Y. Morii, Magnetic and neutron diffraction study on perovskites La_{1-x}Sr_xCrO₃, *J. Solid State Chem.* **141**, 404 (1998).
- [24] M. S. Lee, P. Lyu, R. V. Chopdekar, A. Scholl, S. T. Retterer, and Y. Takamura, Controlling antiferromagnetic domains in patterned La_{0.7}Sr_{0.3}FeO₃ thin films, *J. Appl. Phys.* **127**, 203901 (2020).
- [25] K. H. L. Zhang, Y. Du, P. V. Sushko, M. E. Bowden, V. Shutthanandan, S. Sallis, L. F. J. Piper, and S. A. Chambers, Hole-induced insulator-to-metal transition in La_{1-x}Sr_xCrO₃ epitaxial films, *Phys. Rev. B* **91**, 155129 (2015).
- [26] M. Brahlek, A. R. Mazza, K. C. Pitike, E. Skoropata, J. Lapano, G. Eres, V. R. Cooper, and T. Z. Ward, Unexpected crystalline homogeneity from the disordered bond network in La(Cr_{0.2}Mn_{0.2}Fe_{0.2}Co_{0.2}Ni_{0.2})O₃ Films, *Phys. Rev. Mater.* **4**, 054407 (2020).
- [27] R. Witte, A. Sarkar, R. Kruk, B. Eggert, R. A. Brand, H. Wende, and H. Hahn, High-entropy oxides: an emerging prospect for magnetic rare-earth transition metal perovskites, *Phys. Rev. Mater.* **3**, 034406 (2019).
- [28] J. Nogués and I. K. Schuller, Exchange bias, *J. Magn. Magn. Mater.* **192**, 203 (1999).
- [29] J. Nogués, J. Sort, V. Langlais, V. Skumryev, S. Suriñach, J. S. Muñoz, and M. D. Baró, Exchange bias in nanostructures, *Phys. Rep.* **422**, 65 (2005).
- [30] T. Z. Ward, Z. Gai, X. Y. Xu, H. W. Guo, L. F. Yin, and J. Shen, Tuning the Metal-Insulator Transition in Manganite Films Through Surface Exchange Coupling with Magnetic Nanodots, *Phys. Rev. Lett.* **106**, 157207 (2011).
- [31] E. Maniv, R. A. Murphy, S. C. Haley, S. Doyle, C. John, A. Maniv, S. K. Ramakrishna, Y.-L. Tang, P. Ercius, R. Ramesh, A. P. Reyes, J. R. Long, and J. G. Analytis, Exchange bias due to

- coupling between coexisting antiferromagnetic and spin-glass orders, *Nat. Phys.* **17**, 525 (2021).
- [32] A. N. Dobrynin, D. N. Ievlev, K. Temst, P. Lievens, J. Margueritat, J. Gonzalo, C. N. Afonso, S. Q. Zhou, A. Vantomme, E. Piscopiello, and G. Van Tendeloo, Critical size for exchange bias in ferromagnetic-antiferromagnetic particles, *Appl. Phys. Lett.* **87**, 012501 (2005).
- [33] A. R. Mazza, E. Skoropata, Y. Sharma, J. Lapano, T. W. Heitmann, B. L. Musico, V. Keppens, Z. Gai, J. W. Freeland, T. R. Charlton, M. J. Brahlek, A. Moreo, E. Dagotto, and T. Z. Ward, Designer magnetism in high entropy oxides, [arXiv:2104.05552](https://arxiv.org/abs/2104.05552) cond-Mat Physicsquant-Ph.
- [34] A. P. Ramirez, Colossal magnetoresistance, *J. Phys. Condens. Matter* **9**, 8171 (1997).
- [35] H. Y. Hwang, S.-W. Cheong, P. G. Radaelli, M. Marezio, and B. Batlogg, Lattice Effects on the Magnetoresistance in Doped LaMnO₃, *Phys. Rev. Lett.* **75**, 914 (1995).
- [36] E. Dagotto, T. Hotta, and A. Moreo, Colossal magnetoresistant materials: The key role of phase separation, *Phys. Rep.* **344**, 1 (2001).